AIAA JOURNAL
Vol. 34, No. 8, August 1996

Sensitivity Analysis of the Aeroacoustic Response of Turbomachinery Blade Rows

Christopher B. Lorence* and Kenneth C. Hall†
Duke University, Durham, North Carolina 27708-0300

A method for computing the change or sensitivity of the aeroacoustic response of a cascade to small changes in airfoil and cascade geometry is presented. The steady flow is modeled by the full potential equation, which is discretized using a variational finite element technique. A streamline computational grid is generated as part of the steady solution. Newton iteration is used to solve for the nonlinear steady flow and grid equations with lower-upper (LU) matrix decomposition plus one forward and one back substitution used to solve the resulting matrix equations. Similarly, the unsteady small disturbance flow about the nonlinear mean flow is modeled by the linearized potential equation together with rapid distortion theory to account for vortical gusts. These linearized equations are discretized using finite elements and solved with a single LU decomposition. The sensitivities of the steady and unsteady flowfields to small changes in geometry are computed by perturbing the discretized equations about the nominal solutions. The resulting linear system of equations can be solved very efficiently because the LU factors of the resulting matrix equations are computed as part of the nominal steady and unsteady solution. Results are presented in this paper to show the accuracy and efficiency of the method, and the implications for aeroacoustic design of turbomachinery blades are discussed.

Nomenclature

C = mean flow speed of sound
c = aerodynamic chord of airfoil
c_1, c_2 = constants used to form rotational velocity field
G = blade-to-blade gap
j = $\sqrt{(-1)}$
K_1, K_2 = wave numbers of incident vortical gusts in drift function/stream function coordinate system
k = ratio of specific heats
n = number of Newton iteration
P = mean flow pressure
$\mathcal{P}$ = source term in grid generator used to control grid spacing
p = perturbation pressure
$\mathcal{Q}$ = source term in grid generator used to control grid spacing
R = mean flow density
r = wake displacement
t = time
V = magnitude of mean velocity
w_0 = gust amplitude
x, y = Cartesian coordinates
$\alpha, \beta, \gamma, \delta$ = coefficients in elliptic grid generation equations
Δ = Lighthill's drift function
H, Ξ = grid coordinates
Θ = stagger angle of cascade
ρ_T = total density
σ = interblade phase angle of disturbance
τ = distance along wake
$\hat{\Phi}, \Phi, \phi$ = unsteady potential, steady potential, and perturbation potential, respectively
$\tilde{\phi}, \tilde{\Phi}$ = pressureless potential used to remove singularity from rotational velocity field
Ψ = mean flow stream function
Ω = flow angle
ω = temporal frequency of unsteady flow

Vector and Matrix Quantities

$\boldsymbol{A}$ = matrix approximation of partial differential equation governing unsteady perturbation flow [see Eq. (26)]
$\boldsymbol{b}$ = inhomogeneous part of discretized unsteady potential equations [see Eq. (26)]
$\boldsymbol{M}$ = vector of residuals of grid generation equations
$\boldsymbol{N}$ = vector of residuals of discretized mean flow potential equations
$\boldsymbol{n}$ = unit normal vector to airfoil and wake surface
$\boldsymbol{S}$ = vector describing geometry of cascade
$\hat{\boldsymbol{V}}, \boldsymbol{v}$ = unsteady and perturbation velocities, respectively
$\boldsymbol{X}$ = vector containing position of computational nodes
$\boldsymbol{\Phi}$ = vector containing mean flow potential at computational nodes
$\boldsymbol{\phi}$ = vector containing perturbation potential at computational nodes

Subscripts

Rot = rotor frame of reference
T = total flow quantity
0 = reference position in definition of drift function
∞ = far upstream conditions

Superscripts

R = rotational velocity field
$'$ = sensitivity derivative

Presented as Paper 95-0166 at the AIAA 33rd Aerospace Sciences Meeting, Reno, NV, Jan. 9–12, 1995; received March 2, 1995; revision received March 27, 1996; accepted for publication April 15, 1996.

*Graduate Research Assistant, Department of Mechanical Engineering and Materials Science; currently Aeromechanical Engineer, General Electric Aircraft Engines, One Neumann Way, MD A412, Cincinnati, OH 45215-6301. Member AIAA.

†Assistant Professor, Department of Mechanical Engineering and Materials Science. Member AIAA.

Introduction

BECAUSE of increasingly stringent regulatory requirements, noise continues to be an obstacle to the design and development of modern aircraft engines. Engine noise can be classified as either broadband noise (e.g., a result of jet exhaust mixing) or tonal noise (e.g., produced by fan, compressor, or turbine stages). As the bypass ratio of the engine increases, tonal noise becomes the more important contributor to the total engine noise.[1] The source of tonal noise is nonuniformities or gusts in the flowfield interacting with

rotor and stator blades. These flow nonuniformities arise from inlet distortion, inlet angle of attack, or viscous wakes from upstream blade rows. Several methods are commonly used to reduce tonal noise. The most important noise reduction strategy is the careful selection of blade counts to cut off acoustic modes.[2,3] The strength of the gust may also be reduced by increasing the axial distance between blade rows. In addition, acoustical liners are often installed in the duct to attenuate the sound levels. Although these strategies will continue to be used in future engine designs, new approaches to reducing noise will be needed as the noise constraints become more severe.

Over the past three decades, analyses for predicting the aeroacoustic response of cascades to incident gusts have advanced considerably. Initially, researchers modeled the airfoils in cascades as flat plates and used singularity methods to predict the aeroacoustic response as a result of excitation from acoustic and vortical gusts.[4–6] Smith[5] found that his flat-plate analysis did a good job of predicting the noise generated by a gust for lightly loaded cascades. However, the method could not predict accurately the noise generated by cascades with significant steady loading. More recently, Hanson[7] has found that steady loading plays an important role in the noise produced by multistage machines. Recognizing the importance of steady loading, a number of investigators have used modern computational fluid dynamic (CFD) techniques to calculate the acoustic response of cascades to acoustic, vortical, and entropic fluctuations. For example, Atassi and Grzedzinski[8] and Hall and Verdon[9] have used a linearized potential formulation together with rapid distortion theory to model gust response. Hall and Crawley[10] and Hall and Clark[11] discretized and solved the linearized Euler equations to model cascade/gust interactions.

If the detailed shape of the airfoils in the cascade and the distribution of unsteady surface pressure significantly alter the noise generated in the far field, then it should be possible to alter the noise characteristics of a cascade by modifying the shape of the airfoils. Recently, investigators have developed aerodynamic sensitivity analyses based on modern CFD schemes. These procedures compute the effect small changes in design variables have on the overall flowfield. For example, Taylor et al.[12] and Baysal and Eleshaky,[13] using an analysis based on the nonlinear Euler equations, have computed the effect of modifying the shape of a nozzle on the flow in the nozzle. More recently, the present authors have developed a sensitivity analysis, based on the full potential equation, that is capable of predicting the effect small changes in geometry have on the unsteady aerodynamic flows associated with cascade flutter.[14]

In this paper, a computationally efficient method for computing the sensitivity of the aeroacoustic response of cascades to small changes in blade geometry is presented. Four quantities are computed: the nominal steady flow through a cascade, the nominal unsteady flow as a result of interaction with an unsteady incident gust, the sensitivity of the steady flow to changes in the airfoil and cascade geometry, and the corresponding sensitivity of the unsteady flow. As we will show, once the nominal solutions have been computed, the computational time required to obtain sensitivity solutions is quite small. Also, we use the present theory to redesign an exit guide vane (EGV) for reduced aft radiated sound pressure levels.

Theory

Flowfield Description

The physical system modeled is shown schematically in Fig. 1. A row of EGVs is subjected to unsteady aerodynamic excitation arising from interaction with the viscous wakes from the upstream rotor. In the rotor frame of reference, these wakes are steady. However, in the EGV frame of reference, the wakes appear to be unsteady. The unsteadiness can be decomposed into harmonics with frequencies that are multiples of blade passing frequency (BPF).

In the present analysis, the flow through the EGVs is assumed to be inviscid and two dimensional. (Although viscous mechanisms are responsible for the creation of the wakes, the subsequent interaction with the EGVs is dominated by inviscid effects.) In addition, it is assumed that the unsteadiness in the flow is small compared with the mean flow. Therefore, the flowfield may be decomposed into a nonlinear steady flow plus a linear small disturbance flow. Because the unsteady flowfield is linear, the unsteady response can be analyzed

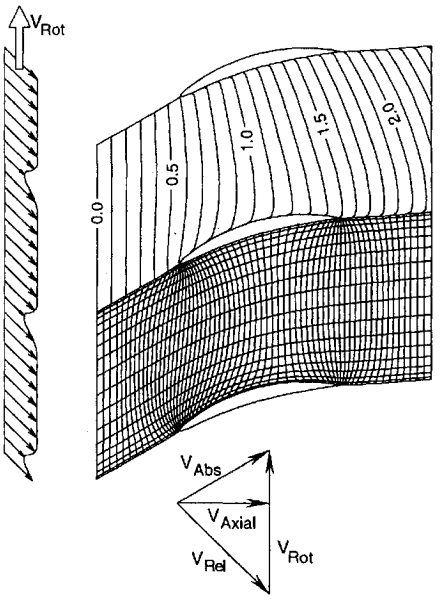

Fig. 1 Schematic showing wake/EGV interaction. Inserts in blade passage show contours of drift (top) and a streamline computational grid (bottom).

harmonic by harmonic, and the results summed together to obtain the complete response. Further, because we are primarily interested in subsonic flows, we assume the steady flowfield is homentropic and irrotational. Thus, we may represent the flowfield by the decomposition

$$\hat{\Phi}(x, y, t) = \Phi(x, y) + \phi(x, y)e^{j\omega t} \tag{1}$$

$$\hat{V}^R(x, y, t) = v^R(x, y)e^{j\omega t} \tag{2}$$

where $\hat{\Phi}$ is a scalar velocity potential, $\hat{V}^R$ is the rotational velocity vector, which contains any vorticity in the flow, and ω is the temporal frequency of the unsteady perturbation flow. Here ϕ and v^R are all small perturbation quantities. Note that we have implicitly assumed that the unsteady flow is homentropic, although entropy variations can be easily incorporated.[8,9]

Substitution of the perturbation assumption, Eqs. (1) and (2), into the conservation of mass and momentum equations, and collection of terms of zeroth and first order in the small perturbation quantities gives the desired steady flow and small disturbance flow equations, respectively. The steady flow is completely described by the steady scalar potential Φ, which can be calculated from the steady full potential equation

$$\nabla^2\Phi = (1/C^2)\left[\tfrac{1}{2}\nabla\Phi \cdot \nabla(\nabla\Phi)^2\right] \tag{3}$$

where C is given by

$$C^2 = C_T^2\left\{1 - \left[(k-1)/2C_T^2\right](\nabla\Phi)^2\right\} \tag{4}$$

where C_T is the stagnation speed of sound. Note that Eq. (3)—which must be solved subject to appropriate boundary conditions on the airfoil, inflow, outflow, and periodic boundaries defining a single blade passage—is nonlinear in the unknown steady velocity potential Φ.

Next, we consider the first-order unsteady small disturbance equations. The unsteady perturbation velocity v is given by

$$v = \nabla\phi + v^R \tag{5}$$

Note that there is no unique choice for v^R and ϕ, because it is the combination of the two that results in the actual unsteady flow velocity. However, in the present investigation, we restrict our choice of v^R so that the unsteady pressure depends only on the unsteady potential ϕ through the linearized Bernoulli equation, i.e.,

$$p = -R\frac{D\phi}{Dt} \tag{6}$$

where p is the unsteady small disturbance pressure, R is the steady density, and D/Dt is the small disturbance substantial derivative operator given by $D/Dt = j\omega + \nabla\Phi\cdot\nabla$. Under these circumstances, the equations governing the small disturbance flow are

$$\frac{D}{Dt}\boldsymbol{v}^R + (\boldsymbol{v}^R \cdot \nabla)\nabla\Phi = 0 \tag{7}$$

$$\frac{D}{Dt}\left(\frac{1}{C^2}\frac{D\phi}{Dt}\right) - \frac{1}{R}\nabla\cdot(R\nabla\phi) = \frac{1}{R}\nabla\cdot(R\boldsymbol{v}^R) \tag{8}$$

Note that because of the judicious choice for the form of the rotational velocity, the equations for the unsteady rotational velocity and velocity potential are only sequentially coupled. Furthermore, as we show in the next section, the rotational velocity $\boldsymbol{v}^R$ can be computed semianalytically using rapid distortion theory.

Rapid Distortion Theory

Goldstein[15] has shown that the rotational velocity $\boldsymbol{v}^R$ can be expressed analytically in terms of two functions: the steady stream function $\Psi(x, y)$ and the steady drift function $\Delta(x, y)$. The drift function[16] is interpreted physically as the time required for a fluid particle to convect between two points on a streamline, that is,

$$\Delta(x, y) = \Delta(x_0, y_0) + \int_{(x_0,y_0)}^{(x,y)} \frac{1}{V}\,d\tau \tag{9}$$

where V is the magnitude of the steady velocity and τ is the distance along the streamline. Goldstein showed that, for the case where an incoming gust varies harmonically in the circumferential direction, the rotational velocity may be expressed as

$$\boldsymbol{v}^R = (c_1\nabla\Delta + c_2\nabla\Psi)\exp[j(K_1\Delta + K_2\Psi)] \tag{10}$$

Goldstein chose the constants c_1 and c_2 so that the rotational velocity in the upstream far field is divergence free and the vorticity of the incoming gust has some prescribed magnitude.

For flows over airfoils with a leading-edge stagnation point (most airfoils), Goldstein's original formulation[15] leads to a singular rotational velocity on the airfoil and wake surfaces because the drift function goes to infinity on the stagnation streamline as the stagnation point is approached [see Eq. (9)]. Atassi and Grzedzinski[8] were able to avoid this difficulty by modifying Goldstein's formulation.[15] Using their approach, the gradient of a convected (and therefore pressureless) potential $\tilde{\phi}$ is added to Goldstein's original rotational velocity. This pressureless potential has the form

$$\tilde{\phi} = \tilde{\Phi}(\Psi)\exp[j(K_1\Delta + K_2\Psi + \omega t)] \tag{11}$$

where

$$\tilde{\Phi}(\Psi) = \frac{j}{K_1}\left\{c_1 + \frac{j\rho_\infty V_\infty G\cos\Omega_\infty(c_2K_1 - c_1K_2)}{2\pi(1 + ja_0K_1)} \times \sin\left[\frac{2\pi\Psi}{\rho_\infty V_\infty G\cos\Omega_\infty}\right]\right\} \tag{12}$$

where ρ_∞ is the upstream steady density, V_∞ is the magnitude of the upstream steady velocity, and Ω_∞ is the upstream inflow angle. The constant a_0 is equal to $-\partial U/\partial n$ evaluated at the stagnation point, where n is the distance from the surface of the airfoil along the stagnation streamline. The quantity $\tilde{\phi}$ has been chosen so that the rotational velocity is zero on the blade and wake surfaces. Consequently, the unsteady rotational velocity can be calculated near the blade and wake surfaces and the singularity in the divergence of the rotational velocity on the blade and wake surfaces is integrable. Finally, the x and y components of the (Atassi and Grzedzinski[8]) rotational velocity can be written as

$$\boldsymbol{v}^R = \left[(c_1 + jK_1\tilde{\Phi})\nabla\Delta + \left(c_2 + jK_2\tilde{\Phi} + \frac{\partial\tilde{\Phi}}{\partial\Psi}\right)\nabla\Psi\right] \times \exp[j(K_1\Delta + K_2\Psi)] \tag{13}$$

Having given the field equations describing the unsteady perturbation flow, we now consider the boundary conditions. The computational domain is composed of a single blade passage bounded by five boundaries: the inflow, outflow, airfoil surface, upstream periodic, and downstream wake/periodic boundaries (see Fig. 1). On the airfoil surface, the normal component of the velocity should be zero. Since in the present formulation the rotational velocity is zero on the airfoil and wake surfaces, the no through flow condition is given by

$$\nabla\phi\cdot\boldsymbol{n} = 0 \tag{14}$$

Similarly, the wake boundaries may be considered no through flow boundaries, but with the additional complication that the wake surface undergoes unsteady oscillations. On each side of the wake, we may write the no through flow condition as

$$\nabla\phi\cdot\boldsymbol{n} = j\omega r + V\frac{\partial r}{\partial\tau} \tag{15}$$

where r is the unknown displacement of the wake normal to the wake's surface. To provide closure for the unsteady wake position r, we apply the condition that the pressure be constant across the wake, i.e.,

$$[\![p]\!] = 0 \tag{16}$$

where $[\![\ldots]\!]$ denotes the jump in the enclosed quantity across the wake.

The original incident gust is assumed to be harmonic in the circumferential direction with circumferential wave number σ/G. The unsteady response to this disturbance will therefore be periodic in the circumferential direction with interblade phase angle σ. Thus, upstream of the airfoil and downstream, the complex periodicity condition

$$\phi(x, y + G) = \phi(x, y)e^{j\sigma} \tag{17}$$

is imposed.

Finally, at the upstream and downstream far-field boundaries, nonreflecting boundary conditions are imposed to prevent spurious reflections of outgoing potential and vorticity waves.[17]

Numerical Solution Technique

Nominal Steady Flow Solver

Now that the governing equations and boundary conditions have been developed, we outline the numerical solution procedure. First, consider the calculation of the steady flow. If only the steady flow potential Φ were required, then Eq. (3) could be discretized on a computational grid and solved subject to appropriate boundary conditions. However, for the unsteady flow calculations, we will also require knowledge of the steady drift and stream functions. It will be useful, therefore, to use a streamline computational grid—that is, a computational grid that has grid lines coincident with the streamlines (see Fig. 1). However, because the streamlines are not known a priori, the location of the grid nodes must be computed as part of the solution procedure.

To generate the computational grid, we use a modified elliptic grid generation technique originally proposed by Thompson et al.[18] The x, y positions of the grid nodes are defined by the partial differential equations

$$\nabla^2\Xi = \mathcal{P} \tag{18}$$

$$\nabla^2 H = \mathcal{Q} \tag{19}$$

where $\mathcal{P}$ and $\mathcal{Q}$ are functions used to control the grid spacing. Lines of constant Ξ and H define the grid lines. We note that the conservation of mass may be expressed as

$$\nabla^2\Psi = \nabla\Phi\times\nabla R \tag{20}$$

Therefore, if we choose $\mathcal{P} = 0$ and $\mathcal{Q} = \nabla\Phi\times\nabla R$, then lines of constant H will correspond to streamlines, provided the boundary conditions around the computational domain are consistent with the definition of the stream function.

As a practical matter, we have found that the influence of the $\nabla\Phi \times \nabla R$ term in Eq. (20) is quite small, at least for the Mach numbers considered in this investigation. That is to say that by neglecting this term, the computational grid lines will not be true streamlines. However, if these quasistreamlines are then taken to be the actual streamlines for the purpose of computing the drift function and rotational velocity [see Eqs. (9) and (13)], then the computed unsteady potential is nearly identical to that computed using the exact streamlines. Therefore, for simplicity and computational efficiency, both $\mathcal{P}$ and $\mathcal{Q}$ in Eqs. (18) and (19) are taken to be zero.

Equations (18) and (19) may be inverted to obtain partial differential equations for the unknown grid node locations in terms of the known computational coordinates Ξ and Ψ (or H), i.e.,

$$\alpha\frac{\partial^2 x}{\partial\Xi^2} - 2\beta\frac{\partial^2 x}{\partial\Xi\partial\Psi} + \gamma\frac{\partial^2 x}{\partial\Psi^2} = -\delta^2(\nabla\Phi \times \nabla R)\frac{\partial x}{\partial\Psi} \tag{21}$$

$$\alpha\frac{\partial^2 y}{\partial\Xi^2} - 2\beta\frac{\partial^2 y}{\partial\Xi\partial\Psi} + \gamma\frac{\partial^2 y}{\partial\Psi^2} = -\delta^2(\nabla\Phi \times \nabla R)\frac{\partial y}{\partial\Psi} \tag{22}$$

where

$$\alpha = \left(\frac{\partial x}{\partial\Psi}\right)^2 + \left(\frac{\partial y}{\partial\Psi}\right)^2, \qquad \beta = \frac{\partial x}{\partial\Xi}\frac{\partial x}{\partial\Psi} + \frac{\partial y}{\partial\Xi}\frac{\partial y}{\partial\Psi}$$

$$\gamma = \left(\frac{\partial x}{\partial\Xi}\right)^2 + \left(\frac{\partial y}{\partial\Xi}\right)^2, \qquad \delta = \frac{\partial x}{\partial\Xi}\frac{\partial y}{\partial\Psi} - \frac{\partial x}{\partial\Psi}\frac{\partial y}{\partial\Xi}$$

Additionally, we must impose boundary conditions around a single blade passage (see Fig. 1). For example, we require that the grid lines corresponding to the stagnation streamlines upstream (and downstream) of the reference airfoil meet the airfoil at the actual stagnation point (and trailing edge). Furthermore, the position of these grid lines must be such that there is no flow through them.

The grid generation equations and associated boundary conditions are discretized using finite difference operators. The resulting set of nonlinear equations is of the form

$$\boldsymbol{M}(\boldsymbol{\Phi}, \boldsymbol{X}; \boldsymbol{S}) = 0 \tag{23}$$

where $\boldsymbol{M}$ is a vector of nonlinear functions, $\boldsymbol{\Phi}$ is a vector containing the discrete approximation of the unknown steady potential Φ at all of the computational nodes, and $\boldsymbol{S}$ is a prescribed vector containing the set of points that define the airfoil shape.

The steady flow equation, Eq. (3), and the associated boundary conditions are discretized using a variational principle and finite element method developed by Hall.[19] In particular, we use four-node isoparametric elements. The resulting discretized equations are nonlinear in the unknowns $\boldsymbol{\Phi}$ and $\boldsymbol{X}$ and have the form

$$\boldsymbol{N}(\boldsymbol{\Phi}, \boldsymbol{X}; \boldsymbol{S}) = 0 \tag{24}$$

In the present study, Eqs. (23) and (24) are solved simultaneously using Newton iteration. The procedure is as follows. First, an initial grid is generated and an initial estimate of the steady solution is made (e.g., uniform flow). Then, we employ the Newton iteration formula given by

$$\begin{Bmatrix}\boldsymbol{\Phi}\\ \boldsymbol{X}\end{Bmatrix}^{n+1} = \begin{Bmatrix}\boldsymbol{\Phi}\\ \boldsymbol{X}\end{Bmatrix}^{n} - \begin{bmatrix}\dfrac{\partial \boldsymbol{N}}{\partial\boldsymbol{\Phi}} & \dfrac{\partial \boldsymbol{N}}{\partial \boldsymbol{X}}\\ \dfrac{\partial \boldsymbol{M}}{\partial\boldsymbol{\Phi}} & \dfrac{\partial \boldsymbol{M}}{\partial \boldsymbol{X}}\end{bmatrix}^{-1}_{n} \begin{Bmatrix}\boldsymbol{N}\\ \boldsymbol{M}\end{Bmatrix}^{n} \tag{25}$$

where n denotes the current estimate of the solution and $n+1$ denotes the new estimate. At each iteration, the matrix in Eq. (25) is not actually inverted. Instead, we factor the Jacobian matrix using lower-upper (LU) decomposition. The LU decomposition routine that we use takes advantage of the block tridiagonal structure of the matrix. Then we solve for the solution at iteration $n+1$ using one forward and one backward substitution. Typically, the Newton iteration procedure converges in about five iterations, and the last LU factors are saved for later use in the sensitivity analysis.

Once the steady flow solution and streamline grid have been obtained, the drift and stream functions must be calculated. Because the grid follows the streamlines, the drift function can be computed very efficiently by discretizing Eq. (9) along streamlines. Furthermore, by construction, each streamwise grid line has a known stream function value. The numerical estimates of the drift and stream functions are stored for later use in the calculation of the unsteady flowfield.

Nominal Unsteady Flow Solver

Next, we consider the solution of the unsteady flow about the cascade arising from interaction with an incident gust. To begin, for a gust of a given frequency and interblade phase angle, we compute the rotational velocity analytically at each of the computational grid nodes using Eq. (13). We then discretize the linearized potential equation, Eq. (8), and its associated boundary conditions on the streamline grid using Hall's finite element procedure[19] along with extensions to include the inhomogeneous vortical term. The resulting discretized equations are linear matrix equations of the form

$$[\boldsymbol{A}]\{\boldsymbol{\phi}\} = \{\boldsymbol{b}\} \tag{26}$$

where the matrix $\boldsymbol{A}$ and the vector $\boldsymbol{b}$ are functions of the mean flow solution $\boldsymbol{\Phi}$, the location of the nodes of the computational grid $\boldsymbol{X}$, and the frequency ω and interblade phase angle σ of the incoming gust. Equation (26) is solved using LU decomposition and again the LU factors are saved for later use.

Note that the only unknowns in the vector $\boldsymbol{\phi}$ are the perturbation potential ϕ at each of the computational nodes, and the position r of the wake at each of the nodes along the wake. Therefore, the number of unknowns in Eq. (26) is approximately one-third the number of unknowns in the discretized steady flow equations.

Once the unsteady potential has been computed, the linearized Bernoulli equation, Eq. (6), is used to compute the unsteady pressure on the surface of the airfoil and in the far field.

Steady Flow Sensitivity Analysis

In this section, we consider the effect of a small change in geometry on the steady flowfield. Consider again Eqs. (23) and (24). If the geometry is perturbed slightly, the perturbed solution will satisfy the equations

$$\begin{Bmatrix}\boldsymbol{N}(\boldsymbol{\Phi}+\boldsymbol{\Phi}', \boldsymbol{X}+\boldsymbol{X}'; \boldsymbol{S}+\boldsymbol{S}')\\ \boldsymbol{M}(\boldsymbol{\Phi}+\boldsymbol{\Phi}', \boldsymbol{X}+\boldsymbol{X}'; \boldsymbol{S}+\boldsymbol{S}')\end{Bmatrix} = 0 \tag{27}$$

where the primed quantities are small perturbation quantities arising from the perturbation in the geometry $\boldsymbol{S}'$. Expanding Eq. (27) in a Taylor series about the nominal solution gives

$$\begin{bmatrix}\dfrac{\partial \boldsymbol{N}}{\partial\boldsymbol{\Phi}} & \dfrac{\partial \boldsymbol{N}}{\partial \boldsymbol{X}}\\ \dfrac{\partial \boldsymbol{M}}{\partial\boldsymbol{\Phi}} & \dfrac{\partial \boldsymbol{M}}{\partial \boldsymbol{X}}\end{bmatrix} \begin{Bmatrix}\boldsymbol{\Phi}'\\ \boldsymbol{X}'\end{Bmatrix} = \begin{Bmatrix}-\dfrac{\partial \boldsymbol{N}}{\partial \boldsymbol{S}}\boldsymbol{S}'\\ -\dfrac{\partial \boldsymbol{M}}{\partial \boldsymbol{S}}\boldsymbol{S}'\end{Bmatrix} \tag{28}$$

The matrices $\partial\boldsymbol{N}/\partial\boldsymbol{\Phi}$, $\partial\boldsymbol{N}/\partial\boldsymbol{X}$, $\partial\boldsymbol{M}/\partial\boldsymbol{\Phi}$, and $\partial\boldsymbol{M}/\partial\boldsymbol{X}$ are large sparse matrices that are determined by linearizing the vectors $\boldsymbol{N}$ and $\boldsymbol{M}$ about the nominal geometry and steady flow. Computation of these matrices is an inexpensive and straightforward process. In addition, there are few entries in the right-hand side of Eq. (28) because only a small number of computational nodes lie on the surface defined by $\boldsymbol{S}$.

To solve for the unknown perturbations $\boldsymbol{\Phi}'$ and $\boldsymbol{X}'$, we rearrange Eq. (28) slightly to obtain

$$\begin{Bmatrix}\boldsymbol{\Phi}'\\ \boldsymbol{X}'\end{Bmatrix} = -\begin{bmatrix}\dfrac{\partial \boldsymbol{N}}{\partial\boldsymbol{\Phi}} & \dfrac{\partial \boldsymbol{N}}{\partial \boldsymbol{X}}\\ \dfrac{\partial \boldsymbol{M}}{\partial\boldsymbol{\Phi}} & \dfrac{\partial \boldsymbol{M}}{\partial \boldsymbol{X}}\end{bmatrix}^{-1} \begin{Bmatrix}\dfrac{\partial \boldsymbol{N}}{\partial \boldsymbol{S}}\boldsymbol{S}'\\ \dfrac{\partial \boldsymbol{M}}{\partial \boldsymbol{S}}\boldsymbol{S}'\end{Bmatrix} \tag{29}$$

Note the similarity of Eq. (29) to Eq. (25). The same matrix must be factored to obtain the perturbed steady solution that was used in the last iteration of the Newton solver. Therefore, since the factored matrix has been saved from the nominal steady flow calculation, the sensitivity quantities $\boldsymbol{\Phi}'$ and $\boldsymbol{X}'$ can be obtained for very little additional computational work.

Unsteady Flow Sensitivity Analysis

Having computed the change in the steady potential as a result of a small change in geometry, we next consider the resulting change in the unsteady potential. The solution of the unsteady flow problem as a result of small changes in the geometry and frequency will be of the form

$$[A(\Phi + \Phi', X + X', \omega + \omega')]\{\phi + \phi'\} = \{b(\Phi + \Phi', X + X', v^R + v^{R'}, \omega + \omega')\} \tag{30}$$

where ϕ' is the unknown sensitivity of the unsteady potential. Expanding Eq. (30) in a perturbation series and collecting terms of first order gives the desired equation for the unknown sensitivity potential ϕ', i.e.,

$$[A]\phi' = \left[\frac{\partial b}{\partial \Phi}\right]\Phi' + \left[\frac{\partial b}{\partial X}\right]X' + \left[\frac{\partial b}{\partial v^R}\right]v^{R'} + \left[\frac{\partial b}{\partial \omega}\right]\omega' - \left[\frac{\partial A}{\partial \Phi}\Phi' + \frac{\partial A}{\partial X}X' + \frac{\partial A}{\partial \omega}\omega'\right]\phi \tag{31}$$

The matrices on the right-hand side of Eq. (31) are large sparse matrices that can be obtained by linearizing the computer code that assembles the matrix A and vector b. Note that X' and Φ' have already been obtained by solving Eq. (29). The perturbation of the rotational velocity $v^{R'}$ can be obtained by analytically perturbing Eq. (9) and Eqs. (11–13). Hence, the right-hand side of Eq. (31) is known. Again, the computational effort required to solve for ϕ' is insignificant because the matrix A has already been factored into upper and lower triangular matrices when the nominal unsteady solution ϕ was computed [Eq. (26)].

Steady and unsteady sensitivity analyses based on the techniques described earlier are computationally very efficient. The computational time required to compute the sensitivity of the steady and unsteady flows to changes in geometry is about an order of magnitude less than the time required to compute the nominal steady and unsteady flows.

Computational Results

To demonstrate the capability of the present method, we analyze in this section a cascade of EGVs typical of those found in modern high-bypass ratio fans. The nominal airfoil shape is a NACA 8508-65 profile. The ratio of the number of fan rotor blades to EGVs, $N_{\text{Rot}}/N_{\text{EGV}}$, is 0.4. In the computational results presented next, lengths are nondimensionalized by the EGV chord c, velocities by the upstream velocity V_∞, frequencies by V_∞/c, pressures by $\rho_\infty V_\infty w_0$, lifts per unit span by $\rho_\infty V_\infty w_0 c$, and moments per unit span by $\rho_\infty V_\infty w_0 c^2$. Here w_0 is the magnitude of the gust velocity normal to the upstream streamlines. A w_0 equal to unity implies the normal velocity would be unity at the leading edge of the reference airfoil at time $t = 0$ if the gust were not distorted. For the case considered here, the gap-to-chord ratio G is 1.0, the inlet Mach number M_∞ is 0.5, the inlet flow angle Ω_∞ is 30 deg, and the stagger angle Θ is 16 deg. The wheel speed of the upstream rotor V_{Rot} is 1.5.

Steady Flow Through a Fan EGV

First, we consider the steady flow through the EGVs. The steady flow was computed using two different H-grids, a 65 × 25 node grid (65 nodes in the streamwise direction and 25 nodes in the normal direction), and a 129 × 49 node grid. Figure 2 shows the nominal steady surface pressure P for this case. For comparison, Fig. 2 also shows the grid-converged solution computed using an Euler solver[11] with a 512 × 65 node grid. The excellent agreement between these three solutions is reassuring and indicates that the steady flow computed using the potential analysis is grid converged. Note that the flow is entirely subsonic.

Unsteady Flow Through a Fan EGV

Next, we consider the acoustic response as a result of viscous wakes from the upstream fan impinging on the EGV. When viewed in the EGV frame of reference, the wake excitation has temporal frequencies $\omega_n = 2\pi n V_{\text{Rot}}/G_{\text{Rot}}$, where V_{Rot} is the wheel speed of the fan, G_{Rot} is the blade-to-blade gap of the rotor, and n takes on all integer values. The corresponding interblade phase angles are $\sigma_n = -2\pi n G_{\text{EGV}}/G_{\text{Rot}}$. The BPF corresponds to $n = 1$ ($\omega_1 = 3.77$ and $\sigma_1 = -144$ deg). At this frequency of excitation, acoustic resonance occurs at interblade phase angles σ of −93.8 and +165.8 deg upstream and −113.0 and +121.9 deg downstream. Thus, the acoustic response of this cascade to excitations at 1 × BPF is cut off; i.e., the unsteady pressure decays exponentially away from the EGVs. However, for excitations at 2 × BPF ($\omega_2 = 7.54$ and $\sigma_2 = -288$ deg), acoustic resonance occurs at interblade phase angles σ of −187.5 and +331.5 deg upstream and −225.9 and +243.8 deg downstream. Therefore, a single acoustic mode with interblade phase angle $\sigma = +72$ deg is cut on in the upstream and downstream regions. Furthermore, the interblade phase angles of the remaining cutoff modes are well separated from the acoustic resonance conditions.

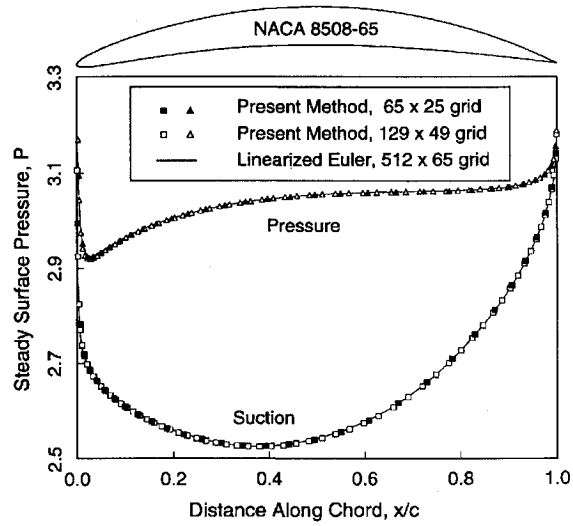

Fig. 2 Steady surface pressure for cascade of NACA 8508-65 EGVs: Θ = 16 deg, Ω_∞ = 30 deg, M_∞ = 0.5, and G = 1.0.

In the following, we consider the acoustic response of the EGV to a 2 × BPF vortical gust with unit amplitude. A unit amplitude gust is one in which the magnitude of the perturbation velocity normal to the upstream flow direction would be unity at the leading edge of the airfoil if the steady flow were uniform and undeflected by the EGV. The real and imaginary parts of the unsteady surface pressure computed using the present analysis, with two different grid resolutions, are shown in Fig. 3. Note that the coarse and fine grid solutions are nearly identical, indicating that the 129 × 49 grid is sufficiently fine to resolve the acoustic behavior of the EGV, at least up to 2 × BPF. Also shown for comparison is the pressure distribution computed using the linearized Euler analysis of Hall and Clark[11] with a 512 × 65 node H-grid. The agreement between the Euler analysis and the present potential/rapid distortion theory is remarkably good, especially considering the high reduced frequency ($\omega = 7.54$). These results demonstrate that the rapid distortion theory has been correctly implemented and that sufficient grid resolution has been used to model unsteady wave propagation.

Figure 4 shows a snapshot of contours of the unsteady perturbation pressure at a given instant in time, $t = 0$ (for this calculation, an extended computational grid is used to more clearly show the outgoing pressure waves). Note the pressure waves radiating away from the cascade upstream and downstream of the cascade. In both the upstream and downstream regions, a single acoustic wave with interblade phase angle of 72 deg is cut on. Also, one observes that the unsteady pressure is somewhat larger in the downstream region than in the upstream region. This is seen more clearly in Fig. 5, which shows contours of the magnitude of the unsteady pressure. The unsteady pressure in the upstream and downstream far-field regions was Fourier transformed in the circumferential direction to determine the magnitude of the single cut-on pressure wave upstream and downstream. For this case, the magnitude of the cut-on unsteady pressure wave (for a unit strength gust) is 0.102 upstream

Table 1 Change in steady and unsteady flow quantities as a result of unit perturbations in 10 design variables

	Steady flow				Unsteady flow: Unconstrained		Unsteady flow: Constrained	
Design variable	L'_y	L'	D'	M'_{LE}	$\lvert p_{up}\rvert'$	$\lvert p_{down}\rvert'$	$\lvert p_{up}\rvert'$	$\lvert p_{down}\rvert'$
Thickness	0.0289	0.0284	0.0059	0.1751	−0.8985	0.2494	−0.9447	0.3099
Maximum thickness location	0.0084	0.0082	0.0017	−0.0164	0.0084	0.0082	−0.0810	0.1161
Camber	1.9254	1.8941	0.3799	−1.6300	0.4441	−1.4103	−6.0899	6.5867
Maximum camber location	0.1991	0.1959	0.0394	−0.2154	−0.1312	0.1224	0.1023	−0.0953
Leading-edge radius	0.0000	0.0000	0.0000	−0.0001	0.0023	0.0023	0.0023	0.0023
Stagger	−0.7558	−0.7266	0.2448	0.0392	−0.3471	0.5910	—	—
Gap	0.3008	0.3220	−0.0313	−0.1123	1.3244	−1.6624	1.4421	−1.8163
Reflex	−2.2190	−2.1827	−0.4387	2.4383	1.8692	−1.5834	—	—
Frequency	—	—	—	—	0.1696	−0.2830	0.1696	−0.2830
Interblade phase angle	—	—	—	—	−0.0822	0.0222	−0.0822	0.0222

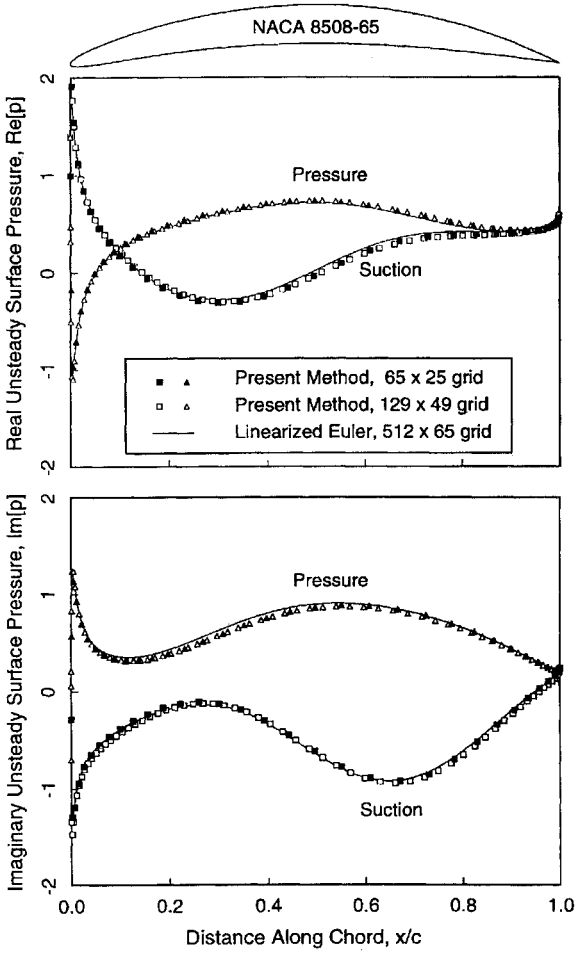

Fig. 3 Unsteady surface pressure for cascade of NACA 8508-65 EGVs as a result of incoming vortical gust at 2 × BPF: ω = 7.54 and σ = −288 deg.

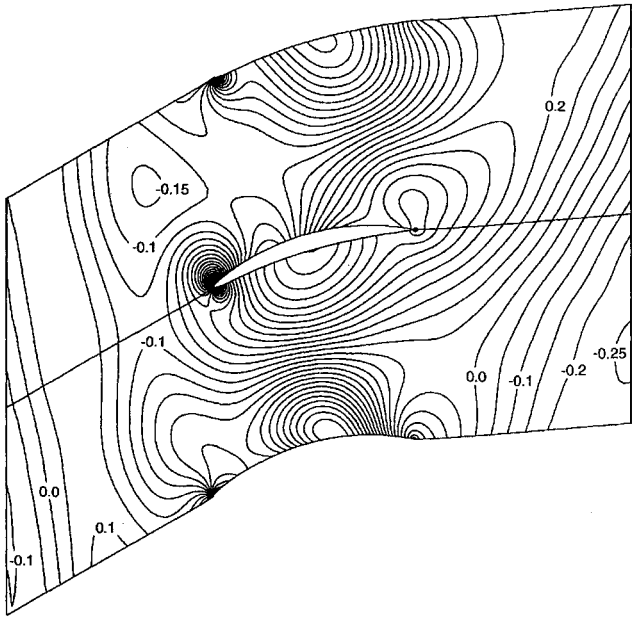

Fig. 4 Contours of instantaneous unsteady pressure for cascade of NACA 8508-65 EGVs as a result of incoming vortical gust at 2 × BPF: ω = 7.54 and σ = −288 deg. Note: extended computational grid used for clarity.

and 0.249 downstream. That is, $p_{up}/(\rho_\infty V_\infty w_0) = 0.102$, where p_{up} is the magnitude of the upstream pressure wave, ρ_∞ is the upstream density, V_∞ is the upstream relative velocity, and w_0 is the gust amplitude.

Sensitivity Analysis

Next, we compute the change in the steady and unsteady aerodynamic behavior and acoustic response as a result of small changes in the EGV geometry. The steady sensitivity analysis was performed using eight different design variables. Five of these variables correspond to the modified NACA definition parameters: thickness, maximum thickness location, camber, maximum camber location, and leading-edge radius. Two design variables define the placement of the airfoils in the cascade: the blade-to-blade gap G and stagger angle Θ. The final design variable is the reflex. For each unit of reflex, one adds to the height of the mean line $c\sin(2\pi x/c)$, where x is now the distance along the airfoil chord.

Using the steady sensitivity analysis outlined in the previous section, we computed the sensitivity of the lift, drag, and moment to changes in the design variables. These results are given in Table 1. The lift and drag are measured normal to and along the chord, and the moment is taken about the leading edge. Also given is the lift L_y in the circumferential direction; L_y is a measure to the steady work done by the cascade. For example, Table 1 indicates that the sensitivity of the nondimensional lift in the circumferential direction to a unit change in camber is 1.9254. Thus, increasing the camber by 3% of the chord will increase the nondimensional circumferential lift L_y by 0.0578.

Table 1 shows that the steady work is most sensitive to changes in camber, reflex, and stagger angle. This is not too surprising because these parameters affect the trailing-edge metal angle of the airfoil and hence the turning (work). On the other hand, the steady turning is relatively insensitive to changes in the maximum thickness location and the size of the leading-edge radius.

Next, we computed the sensitivities of the unsteady pressure to small changes in the design variables for the 2 × BPF case. In addition to the eight design variables described earlier, we include the frequency ω and interblade phase angle σ of the excitation. Figure 6 shows the real and imaginary parts, respectively, of the sensitivity of the unsteady surface pressure to changes in five of these design variables. Also shown for comparison are the sensitivities calculated

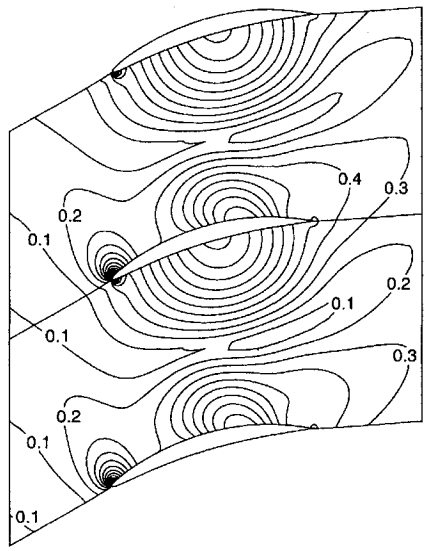

Fig. 5 Contours of magnitude of unsteady pressure for cascade of NACA 8508-65 EGVs as a result of incoming vortical gust at 2 × BPF: $\omega = 7.54$ and $\sigma = -288$ deg.

using a finite difference approach, i.e., the difference of the pressures calculated using the nominal analysis on two slightly different airfoils normalized by the difference in geometry. The nearly exact agreement between the two methods demonstrates that the present sensitivity analysis has been formulated correctly.

Of particular interest in aeroacoustic applications is the influence of the blade shape on the sound radiated upstream and downstream of the EGV. The sensitivity of the magnitude of the cut-on propagating pressure waves to changes in the design variables is given in Table 1. The label "Unconstrained" indicates that each of the design variables is perturbed independently. As an example, the nominal (nondimensional) downstream going pressure wave has a magnitude of 0.249. According to Table 1, the sensitivity of the downstream pressure wave to camber is −1.4103. Hence, increasing the camber by 3% will reduce the nondimensional pressure by 0.0423 or 1.62 dB.

Note that changing the camber also changes the steady work done by the cascade. As a practical matter, if one were redesigning the EGV for reduced noise, one would hold the turning done by the cascade (that is the total work done) fixed to a prescribed value. Also, the steady incidence angle should not change significantly. Thus, we have computed the constrained sensitivity. Each of the design variables is perturbed as before, but the stagger angle and reflex are allowed to float to satisfy the constraints that the steady work and incidence angles remain fixed. Further details of the constraint procedure are given in Ref. 14. Examining the "Constrained" columns in Table 1, we see, for example, that increasing the camber now increases the magnitude of the upstream pressure wave and decreases the magnitude of the downstream pressure wave. The constrained sensitivity is 6.587. Hence, increasing the camber by 3% would increase the pressure by 0.198 or 5.07 dB. Both the gap G and camber are seen to have a strong influence on the strength of the outgoing acoustic waves, although large changes in the gap are aerodynamically more feasible than large changes in camber.

Redesign of an EGV for Reduced Acoustic Response

Next, we used the constrained sensitivities to guide the redesign of the EGV to reduce the sound pressure levels in the downstream region. As previously noted, the camber and gap strongly influence the outgoing pressure waves. Therefore, to reduce the downstream pressure wave, we increase the blade-to-blade gap by 0.1 and decrease the camber by 0.0025. To satisfy the turning and incidence constraints, we must also reduce the stagger angle Θ by 2.23 deg and add 0.0078 units of reflex. Also note that the interblade phase angle σ is decreased from −288 to −317 deg because the interblade phase angle is proportional to the gap. For these design changes, the sensitivity analysis (see Table 1) predicts that the downstream pressure wave will be reduced by 13.8 dB.

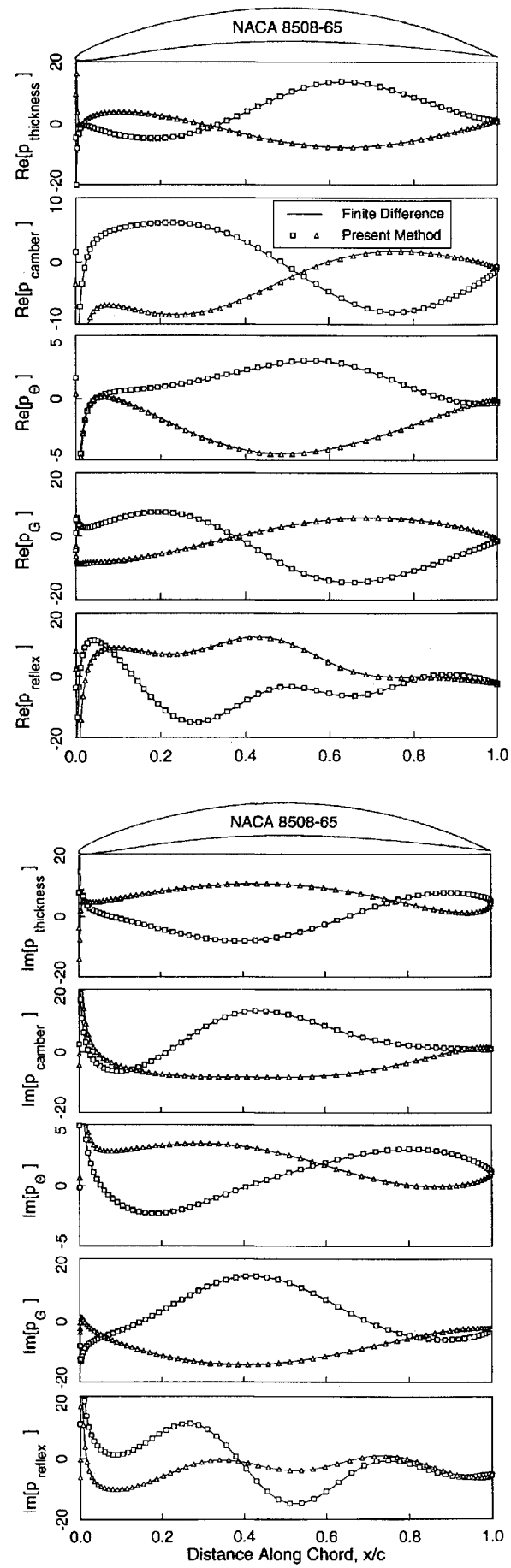

Fig. 6 Sensitivity of unsteady surface pressure on NACA 8508-65 EGVs as a result of perturbations in thickness, camber, stagger, gap, and reflex: $\omega = 7.54$ and $\sigma = -288$ deg. □, suction surface and △, pressure surface.

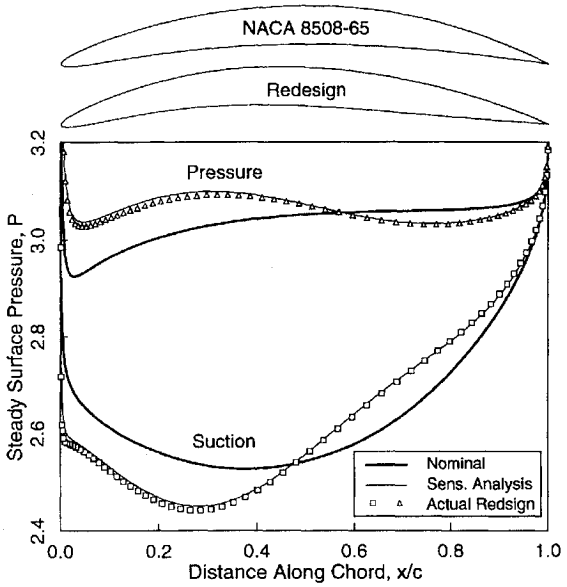

Fig. 7 Steady surface pressure for cascade of redesigned EGVs: M_∞ = 0.5 and Ω_∞ = 30 deg.

Figure 7 shows the nominal and redesigned airfoils and their respective steady surface pressure distributions. The redesigned pressure distribution was computed in two ways: first by linear extrapolation using the design sensitivities and second using the nonlinear steady flow analysis with the actual redesigned airfoil geometry. The good agreement between the two techniques shows that the present steady sensitivity analysis is valid for moderate changes in geometry. Also, one can see in Fig. 7 that the net lift has increased to account for the additional steady work done by each blade because of the increase in blade-to-blade gap.

Figure 8 shows the real and imaginary parts of the unsteady surface pressure for the nominal and redesigned cascade. Note that although the sensitivity analysis correctly predicts the trends of the unsteady pressure distribution of the redesigned EGV, there are some significant differences in the details. The reason for this difference can be demonstrated by examining the effect of the size of the design change. Let us define the design change made here to be a unit change. Figure 9 shows the predicted change in the upstream and downstream sound pressure levels a function of the amplitude of the design change. For small amplitude changes, the sensitivity analysis is seen to be in excellent agreement with the solution computed using the nominal flow solvers with the modified airfoil. However, for design changes near unity, the agreement between the predicted sound pressure levels and the actual sound pressure levels is not as good. These differences are a result of nonlinear effects, that is, effects that to leading order go like the square of the amplitude of the design change. Nevertheless, the sensitivity analysis still gives at least a qualitative prediction of the change in the unsteady pressure distribution on the airfoil and the sound pressure levels in the far field.

Figure 10 shows the unsteady pressure contours for the redesigned cascade. Comparing it with Fig. 5, we note that the downstream pressure levels have been substantially reduced, although the upstream pressure levels have been increased. The magnitude of the downstream pressure wave was reduced about 60%, from 0.249 to 0.099. In acoustic terms, the sound pressure level (SPL) is reduced by 8.0 dB. Upstream, the magnitude of the unsteady pressure is increased from 0.102 to 0.209, an increase of 6.2 dB in the SPL. Looking at the "Unconstrained" columns in Table 1, a change in a design variable usually reduces the magnitude of the noise on one side of the cascade but increases the magnitude of the noise on the other side. Thus, it is difficult in this case to simultaneously reduce the radiated noise both upstream and downstream. We cannot say with certainty why this should be, but we can speculate. A vortical gust carries energy toward the cascade. Energy is carried away from the cascade in the form of vorticity in the field and wake and as

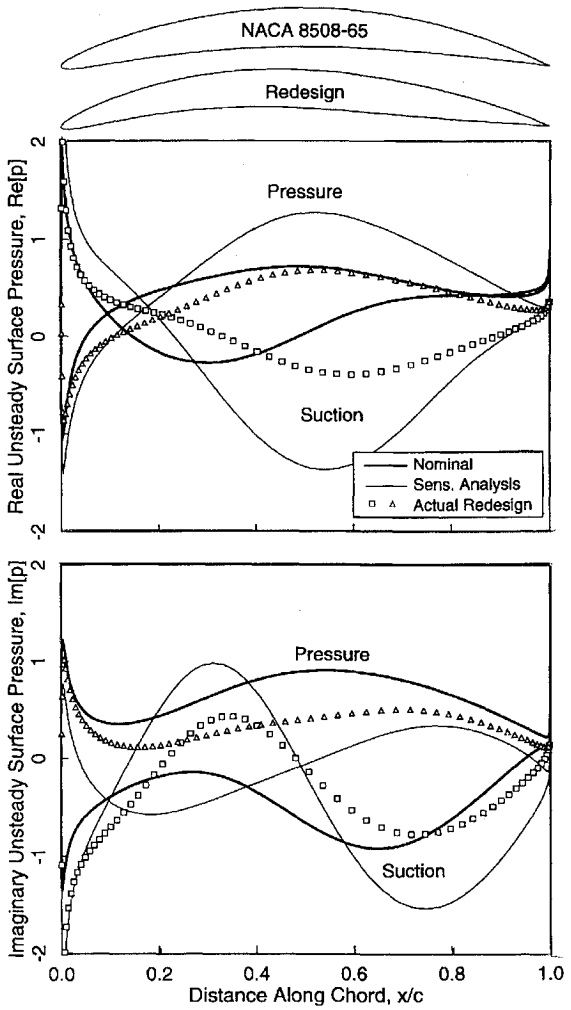

Fig. 8 Real and imaginary parts of unsteady surface pressure for redesigned EGVs as a result of incident vortical gust at 2 × BPF: ω = 7.54 and σ = −317 deg.

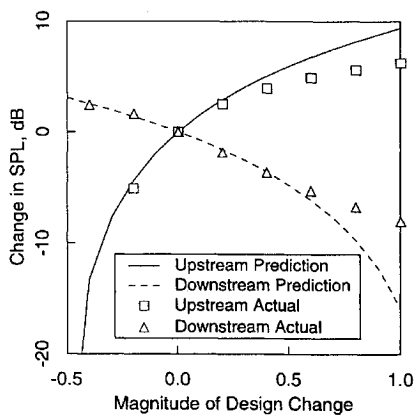

Fig. 9 Accuracy of sensitivity analysis for various perturbation amplitudes.

acoustical energy (pressure waves). Changing the geometry of the cascade is likely to have three effects. First, geometry changes may decrease or increase the energy extracted from the incoming gust. Second, the form of the outgoing energy may be modified; i.e., some of the energy may be converted to shed vorticity instead of acoustic waves. Third, the downstream acoustic energy may be reduced by increasing the upstream acoustic energy. It is thought that the latter is the dominant mechanism at work. Such changes in directivity rely strongly on constructive and destructive interference arising from noncompact acoustic sources. Thus, designs that significantly

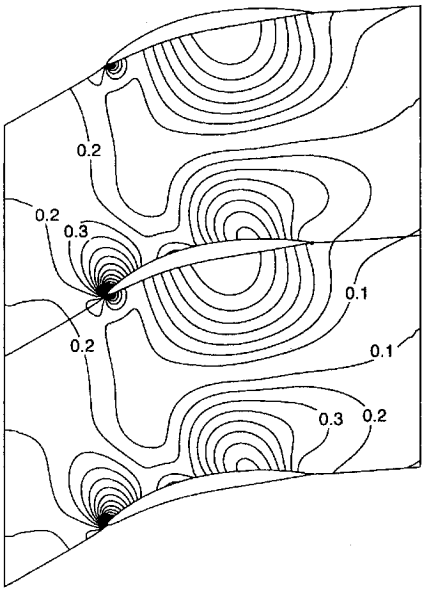

Fig. 10 Contours of magnitude of unsteady pressure for cascade of redesigned EGVs as a result of incoming vortical gust at 2 × BPF: ω = 7.54 and σ = −317 deg.

reduce the noise generated in the downstream region will not necessarily reduce the amplitude of the unsteady blade loads but instead may redistribute the unsteady pressure distribution.

Nor is it immediately obvious why in this case increasing the gap should decrease the aft radiating SPL. In fact, we have found that, at an inflow Mach number M_∞ of 0.3, the SPL in the downstream region is increased with increasing gap. The frequency of excitation is quite high ($\omega = 7.54$), resulting in short wavelength pressure waves. Said another way, the airfoils cannot be considered compact acoustic sources, and therefore constructive and destructive interference effects because of changes in the unsteady pressure distribution on the EGV surface are significant. Thus, it is difficult to sort out intuitively or through simple heuristic models why at a Mach number of 0.5 increasing the gap decreases the noise, and at a Mach number of 0.3 the noise is increased. This is precisely why the present sensitivity analysis is useful: it provides an efficient and systematic way to model the effects of design changes on tonal noise.

Computational Efficiency

Finally, a note about the computational speed of the present method. All computations presented in this paper were carried out on a Silicon Graphics Indigo R4400. The nominal steady flow calculation required 837 s of CPU time, whereas the nominal unsteady computation required 12.8 s. For a single design variable, the steady sensitivity analysis required 3.6 s and the unsteady sensitivity analysis required 6.1 s. Consequently, for the 8 steady and 10 unsteady design variables considered here, the steady sensitivity analysis took 28.8 s of CPU time, whereas the unsteady sensitivity analysis took 61.0 s. For comparison, computing the sensitivity analysis using a finite difference approach would require 13,394 s for the steady calculation and 256 s for the unsteady calculation.

Concluding Remarks

In this paper, a method for calculating the sensitivity of the aeroacoustic response of a cascade to small changes in airfoil and cascade geometry is presented. The steady and small disturbance unsteady flow through the cascade are modeled using the steady and linearized versions of the full potential equation along with rapid distortion theory to model the effect of incident vortical gusts. A variational finite element technique is used to discretize the steady and unsteady flow equations. The discretized steady equations are solved using Newton iteration with LU decomposition. The discretized small disturbances are solved using a single LU decomposition.

The sensitivities of the steady and unsteady flow to changes in design variables are computed in a straightforward fashion by expanding the steady and unsteady flow equations in perturbation series and collecting terms of equal order. The resulting equations for the sensitivities can be solved very efficiently by performing one forward and one back substitution for each design variable using the LU factors obtained from the nominal solutions.

The present sensitivity analysis was used to redesign a typical two-dimensional fan EGV for reduced downstream sound pressure levels. Using this method, a modest but significant 8.0-dB reduction in the magnitude of the sound pressure level in the duct was obtained, but with an accompanying 6.2-dB increase in the sound pressure level upstream. It is likely that such zero sum changes in the sound pressure levels are a result of the limitations imposed by two-dimensionality; that is, the main effect of the design changes is to redistribute acoustic sources on the airfoil surface to produce destructive interference downstream while simultaneously producing constructive interference upstream. Efforts are under way to extend the method to three-dimensional blade rows. It is expected that much larger reductions in sound pressure level both upstream and downstream will be possible by altering the circumferential and axial stacking of the EGVs to redistribute the acoustic sources on the airfoil surface so as to shift the acoustic response from low-order radial duct modes, which are cut on, to high-order radial duct modes, which are cut off.

Finally, it should be emphasized that the present analysis is not a complete noise prediction method; a complete system would include an aft fan duct noise radiation analysis, which models the behavior of acoustic waves as they exit the fan of the engine and interact with the jet, nacelle, and exterior freestream. Nevertheless, because the acoustic problem is linear, reducing the magnitude of the propagating duct modes will generally reduce the radiated sound corresponding to the circumferential mode order by a similar amount. Moreover, the sensitivity analysis described in this paper is quite general and could be easily applied to an aft fan duct noise radiation model.

Acknowledgments

This work was supported by NASA Lewis Research Center, NASA Grant NAG3–1433, with Daniel Hoyniak serving as technical monitor.

References

[1]Gliebe, P. R., "Aeroacoustics in Turbomachines and Propellers—Future Research Needs," *Unsteady Aerodynamics, Aeroacoustics, and Aeroelasticity of Turbomachines and Propellers*, edited by H. M. Atassi, Springer–Verlag, New York, 1993.

[2]Tyler, J. M., and Sofrin, T. G., "Axial Flow Compressor Noise Studies," *SAE Transactions*, Vol. 70, 1962, pp. 309–332.

[3]Morfey, C. L., "Rotating Pressure Patterns in Ducts: Their Generation and Transmission," *Journal of Sound and Vibration*, Vol. 1, Jan. 1964, pp. 60–87.

[4]Whitehead, D. S., "Vibration and Sound Generation in a Cascade of Flat Plates in Subsonic Flow," Aeronautical Research Council, Reports and Memoranda 3685, London, Feb. 1970.

[5]Smith, S. N., "Discrete Frequency Sound Generation in Axial Flow Turbomachines," Aeronautical Research Council, Reports and Memoranda 3709, London, March 1972.

[6]Kaji, S., and Okazaki, T., "Generation of Sound by Rotor-Stator Interaction," *Journal of Sound and Vibration*, Vol. 13, No. 3, 1970, pp. 281–307.

[7]Hanson, D. B., "Mode Trapping in Coupled 2D Cascades–Acoustic and Aerodynamic Results," AIAA Paper 93-4417, Oct. 1993.

[8]Atassi, H. M., and Grzedzinski, J., "Unsteady Disturbances of Streaming Motions Around Bodies," *Journal of Fluid Mechanics*, Vol. 209, Dec. 1989, pp. 385–403.

[9]Hall, K. C., and Verdon, J. M., "Gust Response Analysis for Cascades Operating in Nonuniform Mean Flows," *AIAA Journal*, Vol. 29, No. 9, 1991, pp. 1463–1471.

[10]Hall, K. C., and Crawley, E. F., "Calculation of Unsteady Flows in Turbomachinery Using the Linearized Euler Equations," *AIAA Journal*, Vol. 27, No. 6, 1989, pp. 777–787.

[11]Hall, K. C., and Clark, W. S., "Linearized Euler Prediction of Unsteady Aerodynamic Loads in Cascades," *AIAA Journal*, Vol. 31, No. 3, 1993, pp. 540–550.

[12]Taylor, A. C., III, Hou, G. W., and Korivi, V. M., "Methodology for Calculating Aerodynamic Sensitivity Derivatives," *AIAA Journal*, Vol. 30, No. 10, 1992, pp. 2411–2419.

[13]Baysal, O., and Eleshaky, M. E., "Aerodynamic Design Optimization Using Sensitivity Analysis and Computational Fluid Dynamics," *AIAA Journal*, Vol. 30, No. 3, 1992, pp. 718–725.

[14]Lorence, C. B., and Hall, K. C., "Sensitivity Analysis of Unsteady Aerodynamic Loads in Cascades," *AIAA Journal*, Vol. 33, No. 9, 1995, pp. 1604–1610.

[15]Goldstein, M. E., "Unsteady Vortical and Entropic Distortions of Potential Flows Round Arbitrary Obstacles," *Journal of Fluid Mechanics*, Vol. 93, Pt. 3, Dec. 1978, pp. 433–468.

[16]Lighthill, M. J., "Drift," *Journal of Fluid Mechanics*, Vol. 1, May 1956, pp. 31–53.

[17]Verdon, J. M., "The Unsteady Flow in the Far Field of an Isolated Blade Row," *Journal of Fluids and Structures*, Vol. 3, No. 2, 1989, pp. 123–149.

[18]Thompson, J. F., Thames, F. C., and Mastin, C. W., "Automatic Numerical Generation of Body-Fitted Curvilinear Coordinate System for Field Containing Any Number of Arbitrary Two-Dimensional Bodies," *Journal of Computational Physics*, Vol. 15, July 1974, pp. 299–319.

[19]Hall, K. C., "Deforming Grid Variational Principle for Unsteady Small Disturbance Flows in Cascades," *AIAA Journal*, Vol. 31, No. 5, 1993, pp. 891–900.